Final Technical Report

External Grant Award Number:
G15AP00055
Recipient:
Optim Seismic Data Solutions, Inc.

Principal Investigator:
Satish Pullammanappallil
Optim SDS, 200 South Virginia Street, Suite 560, Reno, NV, 89501
Telephone: (775) 236-5891 Fax :(775) 324-5662 satish@optimsoftware.com

Title:
Determination of Deep Shear-Velocity Structure across the Reno-Area Basin
NEHRP Elements(s)

Element I: National and regional earthquake hazards assessments
Keywords: Site effects, Basin effects, Ground motions, Seismic Zonation, Engineering seismology

Start date: March 2015
End Date: March 2016

Research supported by the U.S. Geological Survey (USGS), Department of the Interior, under USGS award number **G15AP00055**. The views and conclusions contained in this document are those of the authors and should not be interpreted as necessarily representing the official policies, either expressed or implied, of the U.S. Government.

External Grant Award Number **G15AP00055**

Determination of Deep Shear-Velocity Structure across the Reno-Area Basin

Satish Pullammanappallil
Optim SDS, 200 South Virginia Street, Suite 560, Reno, NV, 89501
Telephone.: (775) 236-5891 Fax:(775) 324-5662 satish@optimsoftware.com

Abstract

A collection of sub-basins characterized only roughly by gravity inversions underlies the Reno, Nevada urban area. Existing velocity models are limited in resolution to intervals of 1 km to 3 km. As a result, 3D basin details are currently insufficient for scenario modeling, an essential component of seismic hazard evaluation. A new economic boom and renewed growth and building in northern Nevada make effective hazard evaluation an urgent priority. Trial scenario models run at the University of Nevada, Reno (UNR) for the 2008 Mogul M5 earthquake event are failing to predict recorded ground motions, even to a factor of two. Further development and refinement of the Community Velocity Model (CVM) within the Reno-Carson City urban corridor (RCC) will allow computation of expected shaking from scenario earthquakes affecting these urban areas. Estimation of the basin structure and the shallow shear-wave velocities within it are essential towards achieving accurate simulations to determine sites of strong earthquake ground shaking and damage. Towards this goal we assess shear-wave velocities beneath two 3-km long seismic arrays. The first is located across the north-eastern portion of the Reno-area basin where gravity indicates major sub-basin structure. The second is located where east-dipping sediments in the deepest western Reno-area sub-basin abut a major west-dipping normal fault at the center of the basin, the "Virginia Street" fault. Through this study shear velocity to depths of up to 1000 m were measured using the refraction-microtremor (ReMi) technique with 50 m depth resolution. This was achieved through the deployment of standalone wireless instruments to record ambient urban noise along the two east-west trending arrays. In total 60 instruments, spaced 50 m apart were deployed along each array. The ReMi technique allowed 1D velocity profiles as a function of depth to be obtained along each array. Subsets of 30 instruments were used to obtain a series of 1D velocity-depth sounding from ambient noise recordings. To map depth and characterize lateral velocity heterogeneity beneath each array, these 1D velocity-depth profiles were interpolated to obtain 2D structural representations of shear-wave velocities.

External Grant Award Number **G15AP00055**

Determination of Deep Shear-Velocity Structure across the Reno-Area Basin

Satish Pullammanappallil
Optim SDS, 200 South Virginia Street, Suite 560, Reno, NV, 89501
Telephone.: (775) 236-5891 Fax:(775) 324-5662 satish@optimsoftware.com

NEHRP Elements(s)
Element I: National and regional earthquake hazards assessments
Keywords: Site effects, Basin effects, Ground motions, Seismic zonation, Engineering seismology

1. Introduction

1.1 Objectives:

A key component of local seismic hazard assessment is the estimation or quantification of local site response. Existing hazard estimates for the Reno area provided by the U.S. Geological Survey National Hazard Maps are nominally appropriate for rock sites. This study contributes towards quantifying the adjustments required to account for local site and 3D basin effects. Our efforts in this project allow characterization of the velocity structure beneath a region of the Reno-area basin that has the potential to produce strong ground shaking due to the sediment thickness. Efforts will contribute towards development and refinement of the Western Basin and Range Community Velocity model and the Reno-Carson City urban hazard map. As a result, ground-motion modeling capabilities will be improved, contributing toward the goal of predicting earthquake ground motions in urban areas and other sensitive sites. Such capabilities are essential for seismic hazard evaluation.

Attempts to compute scenario shaking models for earthquakes affecting Reno, point to a crying need for better definition of the geometry of the Reno-area basin and of the velocities within it (Pancha *et al*., 2004). Louie's group at UNR has been building the Nevada ShakeZoning community seismic modeling environment to take advantage of the growing data sets within the Western Basin and Range Community Velocity Model. But current velocity data for the Reno-area basin are limited in resolution to intervals of 1 km to 3 km (Preston and von Seggern, 2007; Tibuleac *et al*., 2009, 2011; Tibuleac personal communication, 2009). Three-dimensional, full-wave synthetic ground motions produced by Nevada ShakeZoning have now been validated for Las Vegas against recordings of the 1992 M5.7 Little Skull Mountain earthquake by Flinchum *et al.* (2012). Figure 1 shows that we have had much less success with trial scenario computations in Reno. Despite trying three different basin models, from Abbott and Louie (2000) as shown in Figure 1, through Saltus and Jachens (1995), to Widmer (2005) and Cashman *et al.* (2012), we have failed to match just the peak ground velocities (PGV)

recorded at most stations in and around the Reno-area basin. Figure 1 (right) illustrates that the data-to-model PGV match is not within even a factor of four. This project obtains shear-velocity sections across the central-eastern region of the Reno-area basin, where little is known about basin depths and velocity structure.

In 2015 Optim SDS and UNR students deployed two seismic arrays, each 2.95 km long, consisting of 60 wireless instruments placed 50 m apart. The locations of these two lines are shown in Figure 2(a) and 2(b). Application of the Refraction Microtremor (ReMi) technique (Louie, 2001) to ambient noise recorded by the arrays resulted in 1D shallow shear-wave velocity profiles to depths of 600 m to 1000 m with 50 m vertical resolution. A series of 1D velocity soundings along each array allowed 2D velocity representations of the shear-wave velocity structure to be created, mapping the near-surface lateral velocity heterogeneity beneath the arrays. This study builds upon the 3D velocity modeling of the deepest western portion of the Reno basin using the ReMi technique under USGS-NEHRP grant award G12AP20026 and in the north-eastern sub-basin under G14AP00020. The locations of these previous five arrays relative to the two arrays deployed in this study are shown in Figure 2(a).

The noisy urban setting, logistics, and high cost mean conventional reflection and refraction studies are impractical for imaging to great depths. Use of wireless stand-alone instruments, together with ambient noise, permits long array data to be inexpensively acquired, allowing velocity characterization of these deep sediments. Our efforts contribute towards improving ground motion modeling capabilities and an accurate understanding of earthquake ground motions and their variability in the Reno area.

1.2 Structure and geology of the Reno-area basin

The Reno-area basin is a fault-bounded graben, with range front fault zones along the western Sierra Nevada margin and an inferred fault bounding the Virginia Range along the eastern side. The west-dipping eastern range-front fault was lately seen first as perhaps the source of the M4.3 Dec. 22, 2015 Thomas Creek earthquake. Two basin-depth models based on gravity data exist for the Reno-area basin. While both the Abbott and Louie (2000) and the Widmer (2005) – Cashman *et al.* (2012) models indicate a similar basin structure within the Reno urban area, both models differ in the absolute depth, and exact structure of this basin. The difference in the basin depths from gravity results from the various definitions and densities of the bedrock basement unit utilized for each geophysical model. The initial model, by Abbott and Louie (2000), defined the volcanic material of the Kate Peak formation as bedrock to modeling basin depth. This is in contrast to Jachens and Moring (1990) who treat the Tertiary Kate Peak volcanics as basin fill, with basement represented by the Cretaceous granite. The new gravity-based models by Cashman *et al*. (2012) incorporate additional gravity data in conjunction with geological constraints from surface observations. Cashman *et al*. (2012) also more robustly defined densities for the nine geological units used in the gravity model. They distinguish between the Tertiary volcanics of the Kate Peak formation at 2.5 g/cc, and the Cretaceous granite and Mesozoic metavolcanics at 2.7 g/cc and 2.8 g/cc respectively.

Recent field mapping combined with seismic reflection imaging and gravity modeling reveal that the east-dipping sediments in the western Reno-area basin abut a major west-dipping normal fault at the center of the basin, the "Virginia Street" fault (Widmer *et al.*, 2007; Cashman *et al.*, 2012; Stephenson *et al.*, 2013), shown in Figure 2. Evidence shows that the "Virginia Street" fault was active during the deposition of gravels which began 2.6 Ma (Trexler *et al*., 2012), as well as throughout the Quaternary (Cashman *et al.,* 2012). Seismic profiles acquired towards understanding the basin structure and fault locations in the area (Stephenson *et al.*, 2013; Frary, 2012) identified the northward extent of the "Virginia Street" fault in addition to newly-recognized faults. Prior to this work, no faults had been recognized in the Reno downtown area (Stephenson *et al.,* 2013). Numerous smaller scale faults also exist within the Reno basin, including a "horst and graben" fault structure discussed by Widmer (2005), which require better characterization.

2. Array configuration and data acquisition:

The objective of the array deployment was to obtain shear-wave velocity information down to 1000 m depth with a depth resolution of 50 m across the central and eastern parts of the basin (Figure 3). Two orthogonal arrays, 2.95 km long, were installed, as shown in Figure 2. The selected line locations best capture the basin-depth variations and the velocity changes across the basin structure. Each array consisted of 60 wireless instruments, spaced 50 m apart. These standalone Sigma™ cableless acquisition systems manufactured by iSeis (Heath, 2011), shown in Figure 4, were paired to standard vertical geophones with natural frequency of 4.5 Hz. Each seismometer unit location was surveyed using a TopCon GRS-1 mobile handheld unit. Once deployed, and powered on, the Sigma™ units started recording passive data. Each Sigma™ unit has its own built in memory, so data is stored on each unit independently. The units record seismic motions continuously, saving the data in one-minute records. Each array was deployed for a total time duration of three hours, using a sampling rate of 2 milliseconds, recording ambient noise. After completion of recording each day, the data was downloaded from each unit, and the one-minute data intervals were concatenated into section records for each line.

Use of wireless stand-alone instruments together with ambient noise enabled data acquisition from long arrays, inexpensively, with limited manpower. However, the urban environment necessitated the need for constant security monitoring of the instruments throughout the deployment, placing constraints on the maximum time span of recording due to personnel budget restrictions.

3. Dispersion curve analysis and shear-wave velocity modeling:

The Refraction Microtremor (ReMi) (SeisOpt® ReMi™, ©Optim 2001-2016) method was used to obtain a series of 1D velocity profiles as function of depth from the noise records captured by the two array lines shown in Figure 2(a) and 2(b). Shallow shear wave velocities are characterized along the arrays using the ReMi technique developed by Louie (2001). The essence of the technique is that ambient noise contains a usable signal that is predictable from the

velocity structure. The ambient noise is dominated by Rayleigh waves initiated by vehicle traffic, overhead airplanes, trains, and other sources. The vertical component of ambient noise, dominated by Rayleigh waves, is recorded by a linear array of geophones usually with equal spacing between each instrument. These Rayleigh waves are separated from other wave arrivals using a two-dimensional slowness–frequency (p–f) transform of the noise records. Figure 5, illustrates the procedure. The noise recordings along the array (Figure 5A) are transformed into a slowness–frequency (p-f) spectrum. The fundamental-mode phase-velocity Rayleigh wave dispersion curve is picked along the minimum-velocity of the envelope of the energy within the slowness–frequency spectral image (Figure 5B). The spectrum is normalized as the ratio of the power spectrum at a particular frequency and slowness (inverse velocity) over the average value for all slowness values at that frequency. This fundamental-mode Rayleigh-wave dispersion curve is then interactively modeled, using trial-and-error adjustments of the velocity model (Figure 5C), to obtain a shear-wave velocity versus depth profile (Figure 5D) that produces a dispersion curve that matches the observed picks. Refraction microtremor is a volume-averaging surface-wave measurement, averaging velocities where geology is laterally variable, thus differing from single point data obtained from downhole logs.

For the Deep ReMi method applied in this study, microtremor data from subsets of consecutive instruments are transformed into slowness–frequency (p-f) space, and a dispersion curve is manually picked along a minimum-velocity envelope where the gradient of the power spectral ratio is greatest (Louie, 2001; Pancha *et al*., 2008) (e.g. Figure 6(B), Figure 7(B), and Figure 8(B)). Forward modeling of the dispersion (e.g. Figure 6(A), Figure 7(A), and Figure 8(A)), curve produces a shear-velocity-*vs.*-depth profile for each sub-array such as that illustrated in Figure 5(C), Figure 6(C), Figure 7(C), and Figure 8(C). These velocity-depth soundings can be vertically averaged to the single Vs30 value used by the NEHRP-UBC code. To characterize and map the lateral velocity heterogeneity beneath the area, the series of 1D velocity-depth profiles are and then interpolated to obtain a 2D structural representation of shear-wave velocities. In essence, the 2D image is comprised from a moving array of instruments.

For the current array data, subsets of 30 consecutive geophone instruments used to produce a series of 1D shear-wave velocity depth profiles characterizing average the shallow structure and basin depths beneath each array. These “sub-arrays” were spaced along each array, nominally moving two instruments along each line. Where significant changes in the 1D velocity profiles were noted, additional sub-arrays were analyzed to adequate characterize structural changes along the length of each line. Table 1 and Table 2 lists the instrument subsets used to obtain 1D velocity soundings along Line 1 and Line 2 from this study respectively.

Ability of the seismic array to image velocity structure at depth depends on the capability of the array to capture ground motion at wavelengths that sample the target depths. The frequency content of the recorded data is dependent on several factors. These include the array length, geophone spacing, sampling rate, geophone frequency, the time length of the data records, and the frequency content of the excited noise sources producing the recorded ground motions. Typically, the depth of penetration of the recorded wave field is half the array length. To successfully image the velocity profile of the entire sediment package and define the basin depth, time length of the recorded ambient noise required to successfully image Rayleigh-wave dispersion at low frequencies representative of the velocity structure at depth. Based on the

results from the study undertaken through under USGS-NEHRP grant award G12AP20026, we utilized the station spacing to 50 m intervals, and used two minute records for the data analysis to best image the Rayleigh-wave dispersion. Through visual inspection of the ambient noise records, the most favorable record sections with high energy waves were selected for analysis. The combination of closer station spacing and record lengths of two minutes, the resultant dispersion curves are much clearer. The introduction clarity of the dispersion images are illustrated in Figures 5 through to Figure 8, where dispersive energy is clearly observed frequencies between 0.5 Hz to 6 Hz.

The reference velocity structure employed for the analysis of data under award G12AP20026 reference models was used to model the shear-velocity structure beneath the central-eastern basin. The maximum velocity of the bedrock basement of the G12AP20026 study was constrained to values consistent with the deeper velocity structure obtained by Preston and von Seggern (2007) through 3-D P- and S-wave tomograhpic inversion. Use of the G12AP20026 reference velocity-depth profile helped restrict bedrock depths and allow determination of the shallower velocity structure. Depths to the high-velocity bedrock interface are resolved by the dispersion picks.

Velocity models for adjacent sub-arrays along each line were adjusted so that while layer velocities remained relatively unchanged, interface depths were modified. Small adjustments of the layer velocities and the of additional layer interface help match the dispersion curve data where needed. The restriction of layer velocities enhanced the ability to map lateral changes in the velocity structure along each line, and to interpolate these changes across the study area to the perpendicular array.

The preferred profile will always be the profile interpretation that results in the minimum number of layers to accommodate the observed Rayleigh-wave dispersion and produces a best estimate, reliable and repeatable velocity structure. Because forward modeling is used rather than an inverse method to obtain our velocity-depth models, we are able to test the necessity and sensitivity of the data to both layer thickness and layer velocity.

4. Results

Analysis of the ambient noise recorded by the two arrays beneath the northwestern sub-basin achieved the goal of characterizing shear-wave velocities in the upper 1 km of the surface and determining the basin structure. The 2D shear-wave representations presented in this section provide a better depiction of the basement topography and major velocity variations than previously available.

Two alternate models of the 2D velocity representation below Line 1 are shown in Figures 9 and 10 respectively. Both show a shallowing of the bedrock depth near the center of the array. Along Line 1, Model 1 has a constant bedrock depth of approximately 365 m beneath much of the array, but shallows to approximately 285 m depth between 1350 m and 1850 m distance. Beyond 1850 m distance, bedrock depth is relatively constant at 320 m – 330 m depth. In comparison, Line 1, Model 2 shows a relatively constant bedrock depth of ~350 m up to 1350

m distance, where the bedrock then shallows to approximately 280 m depth, before returning to a constant depth of 340 m at a distance of 1815 m to 1915 m along the array.

Splayed faults of the Mount Rose Fault system (Sawyer, 1999) are shown to transect the Line 2 seismic array. The two major branches shown in Figure 2, form a topographically expressed graben to the north of the array, and intersect Line 2 between 1720 m and 1870 m from the western end of the array. These faults align with the major west-dipping normal fault at the center of the basin, the "Virginia Street" fault (Widmer *et al*., 2007; Cashman et al., 2012; Stephenson *et al.,* 2013). Across Line 2, no distinct topographic expression of the faults is apparent. Beneath Line 2, three alternate 2D velocity models were developed using the moving array ReMi analysis technique, and are presented in Figures 11, 12, and 13. All three show a relatively smooth basin bottom from 720 m distance to1850 m, with a basement depth of 500m to 550 m depth. Differences in the three models developed for Line 2 occur to the east of the 1850 m distance location. Model 1 shows a progressive stepping to shallower depths from 500 m to 400 m at 1850 distance, and then to 350 m depth at 1950 m distance. Model 2 displays an abrupt decrease in basement depth from 520 m at 1600 m distance to 435 m depth at approximately 1650 m distance. This is followed by another decrease to 370 m depth which occurs at 1850 distance. A more abrupt change from 500 m to 370 m basement depth occurs at 1850 m distance in Model 3. These three models beneath Line 2 demonstrate that the Rayleigh-wave dispersion data are not conclusive to resolve the exact structure. Nevertheless, the three models presented in Figures 11, 12, and 13 reveal the approximate location and nature of the edge of the western most sub-basin east-dipping sediments abut a major west-dipping normal faults at the center of the basin. The consistent offset of the basement depth at 1850 m distance coincides with the surface trace of the eastern splay of the Mt Rose fault system (Sawyer, 1999) shown in Figure 2. Moreover, the offset at approximately 1650 m may delineate the subsurface projection of the western splay located at 1745 m distance on the surface by Sawyer (1999), which defines the edge of the graben further to the north. The fault interaction of the two splays at the location of Line 2, may express a convergence zone between the graben to the north, and the extensional Virginia Lake 1,000 m to the south.

5. Contribution towards seismic hazard assessment and ground motion prediction

One major question confronting the assessment of earthquake hazard within the entire Reno-area basin is whether or not the thick (~2 km) Kate Peak deposits act like basin sediments, with the Cretaceous granite beneath acting as the true bedrock from a seismic response point of view. Our deep velocity characterization combined with scenario earthquake modeling can address this issue. Abbott and Louie (2000) defined the volcanic material of the Kate Peak formation as bedrock to modeling basin depth. The new gravity-based models by Cashman *et al*. (2012) distinguish between the Tertiary volcanics of the Kate Peak formation, the Cretaceous granite, and Mesozoic metavolcanics, as discussed above, in their modelling of the gravity anomaly across the basin. Comparisons between basin depths derived from the two gravity studies and the ReMi analysis models along the two seismic arrays are presented in Figure 14.

Along Line 1, the Cashman *et al.* (2012) gravity basement model very closely mimics Model 1 derived in this study. This close agreement suggests that for this area of the basin, the Kate Peak deposits are not as extensive in thickness as previously thought within this sub-basin, with a lower density material, correlating with the lower velocity basin sediments shown in Figures 9 and 10. In comparison the gravity basin depths determined by Abbott and Louie (2000) are on the order of 200 m to 250 m deeper.

In contrast, along Line 2, the Abbott and Louie (2000) gravity model appears to underestimates the basin depth by ~300 m, compared to the results of this study. The Cashman *et al.* (2012) basin depths are approximately 150 m to 200 m shallower than those derived from the ReMi analysis, but the basin shape mimics the changes in basin depth determined from the Rayleigh-wave dispersion data. The differences presented in Figure 14(b) highlight the differences in the interpreted basin structure, basin fill, and definition in basement lithology in this region. More work is required along this eastern edge of this western sub-basin to characterize the juxtaposition of sediments against the faults blocks defining this margin. As seen from Figures 11, 12, and 13, the basement structure in this region is complex.

Aside from characterization of basin structure, results of this study also help identify areas susceptible to shaking during large earthquake events due to near-surface shear-wave velocity and basin depth. Efforts of this study contribute towards development of the Western Basin and Range Community Velocity model and the Reno-Carson City urban hazard map. The final step will be the incorporation of the basin and shear-wave velocity structure into the Nevada ShakeZoning community seismic modeling environment at the Nevada Seismological Laboratory at the University of Nevada, Reno. This will aid improvement in ground-motion modeling capabilities contributing toward the goal of predicting earthquake ground motions in this highly populated and earthquake prone urban region.

Towards assisting development and implementation of the next generation attenuation (NGA) models, using the 1D velocity sounding along each site, values of average velocities Vs30, Vs50 and Vs100 to depths of 30, 50, and 100 meters are computed by arithmetic slowness averaging with the formula below:

$$VsZ = \frac{Z}{\sum_{1}^{N} \frac{z_i}{V_i}}$$

where Z is the total depth, z_i is the thickness of layer i with shear velocity V_i. Similarly, we have picked Z0.5, Z1.0, Z1.5, and Z2.0, which are the depths where the shear velocity first exceeds 0.5 km/s, 1.0 km/s, 1.5 km/s, and 2.0 km/s respectively. These values are listed in Table 1(a)-(b) and Table 2(a)-(c). Caution however must be used when using the Vs30 values reported in Table 1 and Table 2. The large station spacing means that velocities above 50 m depth are not well resolved. To obtain reliable velocity estimates using ReMi in this depth range, additional arrays with closer station spacing are required. The shorter array lengths allow denser measurements to characterize the near-surface, which likely exhibits greater velocity variations.

6. Conclusions:

Analysis of the ambient noise record recorded by the two arrays presented in Figure 2 successfully achieved the goal of refinement the basin structure and characterization of shear-wave velocities in the upper 1 km of the surface. The 2D shear-wave representations presented in Figures 9 through Figure 13 provide a more accurate depiction of the basin shape than previously available. Future studies within the Reno-area basin will benefit from this knowledge, allowing subsequent arrays to be ideally places to improve our knowledge of the basin structure and the velocities within it. While small scale near-surface faults may be present in the upper 50 m, which may manifest appreciable velocity contrasts, due to the station spacing of 50 m, these are not able to be characterized by this study. Array lengths with denser measurements are required to characterize the near-surface.

7. Future work: Further constraint of the models:

One possible caveat of these shear-wave velocity models is the trade-off between velocity and depth. We propose to refine the 2D velocity models through use of cross-correlation and auto-correlation of the ambient noise records to image the geological structure beneath the arrays. Using seismic interferometry through cross-correlation and auto-correlation the P reflection time section from the ambient noise records is recovered. Stacking of these results over time windows will allow generation of a virtual shot gather. Processing of these virtual shot gathers will result in an image of the Earth's reflection response beneath each of the three arrays. Seismic interferometry has been tested through a pilot study with comparison of active source data across two seismic lines gathered in Nevada. Ambient noise data were recorded over three consecutive days at sensors co-located along the location of two active seismic reflection array lines. Comparison of processed noise cross-correlation data with the traditional active seismic reflection record sections show encouraging similarities (Tibuleac *et al.*, 2010). One downfall of that pilot study was the lack of surface ambient noise and poor azimuthal coverage of noise sources. The urban setting of the data analyzed under this proposal overcomes these data limitations, enhancing the potential of obtaining detailed seismic reflection images.

To further test the abilities of the seismic interferometry technique, a seismic investigation was conducted along Hadfield Road, Kapiti, New Zealand, over a fault trace imaged by an air photo taken in April 1948. Ambient noise within this urban area was recorded over the location and both 2D ReMi and seismic interferometry analyses were conducted. A preliminary depth-migrated section of the virtual shot gathers is presented in Figure 15(a). Comparison with preliminary depth-migrated section with a 2D velocity-depth structural representation compiled using 2D ReMi analysis beneath the array. The 2D velocity-depth representation was created blindly without consultation of the final depth-migrated section of the virtual shot gathers. The 2D velocity profile constructed using the moving-array ReMi technique was able to determine velocity interfaces that match well with changes in material properties that are evident within the depth-section presented in Figure 15(a). The good correlation between the velocity interfaces and the observed textural changes relating to differences in material properties in the depth-section gives us confidence that such analysis of the data from USGS-NEHRP grant awards G12AP20026, G14AP00020, and G15AP00055 (this report) will provide

vital information to help improve the 3D basin model of the Reno area. Images, such as that presented in Figure 15(a) would help delineate the nature of the off-set basement structure on Figures 11, 12, and 13, highlighting the position of the west dipping faults and graben structure

Noise sources from the urban setting of the data from this study will provide detailed waveform data to image subsurface structure. The abundant cultural noise from all azimuths, make this data ideal and affords us a unique opportunity to apply this new imaging method. Depths to prominent material interfaces with high impedance contrasts can be identified from these sections, including the basin bottom. These depths will place additional constraints on the forward modeling of the Rayleigh-wave dispersion data used to invert for the velocity-depth structure beneath each array. The resultant seismic interferometric reflection images may also highlight the existence and location of localized faulting in the area along with other geological features such as discontinuities..

8. Acknowledgements:

We thank Dr. John Louie and his team of students for their help with field deployment, and monitoring of the seismic instruments. We also wish to thank Dr. Aasha Pancha who assisted with the ReMi analysis and interpretation.

9. References:

Abbott, R. E., and J. N Louie. (2000). Depth to bedrock using gravimetry in the Reno and Carson City, Nevada area basins, *Geophysics*, 65, 340-350.

Cashman, P. H.,J. H. Trexler, Jr., M. C. . Widmer, and S. J. Queen (2012). Post–2.6 Ma tectonic and topographic evolution of the northeastern Sierra Nevada: The record in the Reno and Verdi basins *Geosphere*, v. 8, p. 972-990, doi:10.1130/GES00764.1.

Clark, M., J. Louie, A. Pancha, J. Scott, and K. Heath (2005). Geophysical investigation of a fault as a hydrologic barrier in Reno, Nevada: presented at the Seismol. Soc. of Amer. Ann. Mtg., Lake Tahoe, Nevada, April 26-29.

Flinchum, B. A., W. H. Savran, K. D. Smith, J. N. Louie, S. K. Pullammanappallil, and A. Pancha, (2012). Validation of Las Vegas basin response to the 1992 Little Skull Mtn. earthquake as predicted by physics-based Nevada ShakeZoning computations, presented at *Seismological Society of America Annual Meeting*, San Diego, April 17. On line at: http://crack.seismo.unr.edu/ma/validation/Flinchum-SSA12.html

Frary, R. N., J. N. Louie, W. J. Stephenson, J. K. Odum, L. Liberty, S. Pullammanappallil, N. Prina, P. Cashman, J. Trexler, and R. L. Kent (2001). 3D Controls on Basin Structure from a Network of High-Resolution Seismic Imaging Profiles in South Reno, Nevada, *Abstract, Sesimological Research Letters*, 82(2), 298, presented at the *Seismological Society Annual Meeting*, 13-15 April, Memphis, Tennessee.

Heath, R. (2011). Time to consider the practicalities of passive seismic acquisition, *First Break*, 29 (7), 91-98.

Louie, J. N. (2001). Faster, better: Shear-wave velocity to 100 meters depth from refraction microtremor arrays, *Bull. Seism. Soc. Amer.*, ***91***, 347-364.

Pancha, A., J.G. Anderson, J.N. Louie, and A. Anooshehpoor (2004). Data and simulation of ground motion for Reno, Nevada, 13th World Conference on Earthquake Engineering, Vancouver, B.C., Canada, Aug. 1-6, 2004, Paper No. 3452.

Pancha, A., J. G. Anderson, J. N. Louie, S. Pullammanappallil, (2008).Measurement of shallow shear wave velocities at a rock site using the ReMi technique, *Soil Dynamics and Earthquake Engineering*, 28, 522-535.

Preston, L., and D. von Seggern (2008), Joint Seismic Tomography/Location Inversion in the Reno/Carson City Area, *Final Report to the National Earthquake Hazard Reduction Program*, U. S. Geological Survey Award Number 07HQGR0022.

Saltus, R. W., and R. C. Jachens (1995). Gravity and basin-depth maps of the Basin and Range Province, Western United States, U.S. Geological Survey, *Geophysical Investigations Map, Report: GP-1012*, 1 sheet.

Sawyer, T.L., compiler, (1999). Fault number 1647, Mount Rose fault zone, in Quaternary fault and fold database of the United States: U.S. Geological Survey website, http://earthquakes.usgs.gov/regional/qfaults, accessed 10/23/2012 05:42 PM.

Stephenson, W. J., R. N. Frary, J. N. Louie, and J. K. Odum (2012). Extensional growth faulting beneath Reno, Nevada, imaged by urban seismic profiling, [in review].

Tibuleac, I. M., D von Seggern, J Louie and J Anderson (2009). High resolution seismic velocity structure in the Reno basin from ambient noise recorded by a variety of instruments, *Geothermal Resources Council 3rd Annual Meeting*, Oct 4-7, 2009, Reno NV, U.S.A.

Tibuleac, I.M.; Pullammanappallil, S.; von Seggern, D. H.; Pancha, A.; Louie, J. N., (2010). Retrieval of Earth's reflection response from ambient seismic noise - a Nevada experiment, *American Geophysical Union, Fall Meeting 2010*, Abstract #S33A-2071

Tibuleac, I. M., D. H. von Seggern, John G. Anderson and J.N. Louie, 2011. Computing Green's Functions from Ambient Noise Recorded by Narrow-Band Seismometers, Accelerometers, and Analog Seismometers, *Seism. Res. Lett*., 82, 661-675. doi: 10.1785/gssrl.82.5.661 http://crack.seismo.unr.edu/ileana/GF ambient noise paper final.pdf

Widmer, M. (2005). Gravity-based geological modeling of the Central Truckee Meadows, prepared for The Central Truckee Meadows Remediation District, Washoe County Department of Water Resources.

Widmer, M. C., Cashman, P. H., Benedict, F. C., and J. H. Trexler (2007). Neogene through Quaternary Stratigraphy and Structure in a Portion of the Truckee Meadows Basin: A Record of Recent Tectonic History, presented at the *Geological Society of America Cordilleran Section*, 103rd Annual Meeting.

10. Tables and Figures

Table 1(a): Instrument groupings used to obtain 1D shear-wave velocity soundings along Line 1, Model 1 (see Figure 2 for location). Average velocities to 10-, 30-, 50-, and 100-meter depths, denoted Vs10[§], Vs30[§], Vs50, and Vs100, respectively are listed along with the depths where the shear velocity first exceeds 0.5 km/s, 1.0 km/s, 1.5 km/s, and 2.0 km/s (Z0.5, Z1.0, Z1.5, and Z2.0 respectively).

Station Spread	Midpoint		Velocity, m/s			Depth, m			
	Latitude	Longitude	Vs30[§]	Vs50	Vs100	Z0.5	Z1.0	Z1.5	Z2.0
Line1 01 to 30	39.5276	-119.7462	366.86	366.86	402.68	72.50	365.00	365.00	365.00
Line1 02 to 31	39.5276	-119.7455	366.86	366.86	385.57	85.00	365.00	365.00	365.00
Line1 03 to 32	39.5276	-119.7450	361.20	361.20	394.10	75.00	365.00	365.00	365.00
Line1 05 to 34	39.5276	-119.7438	361.20	361.20	394.10	75.00	370.00	370.00	370.00
Line1 07 to 36	39.5276	-119.7426	361.20	361.20	390.54	77.50	370.00	370.00	370.00
Line1 09 to 38	39.5276	-119.7415	338.57	338.57	385.65	67.50	365.00	365.00	365.00
Line1 11 to 40	39.5276	-119.7403	338.57	338.57	381.88	72.50	352.50	352.50	352.50
Line1 13 to 42	39.5275	-119.7391	349.88	349.88	390.47	75.00	315.00	315.00	315.00
Line1 15 to 44	39.5275	-119.7380	378.18	378.18	404.24	82.50	315.00	315.00	315.00
Line1 17 to 46	39.5275	-119.7368	395.15	395.15	405.49	92.50	282.50	282.50	282.50
Line1 19 to 48	39.5274	-119.7357	412.12	412.12	432.01	82.50	282.50	282.50	282.50
Line1 21 to 50	39.5274	-119.7345	417.78	417.78	417.78	100.00	320.00	320.00	320.00
Line1 23 to 52	39.5273	-119.7333	412.12	412.12	415.36	97.50	320.00	320.00	320.00
Line1 25 to 54	39.5273	-119.7322	417.78	417.78	417.78	100.00	327.50	327.50	327.50
Line1 27 to 56	39.5274	-119.7310	417.78	417.78	417.78	125.00	330.00	330.00	330.00
Line1 29 to 58	39.5274	-119.7299	417.78	417.78	417.78	125.00	330.00	330.00	330.00
Line1 31 to 60	39.5274	-119.7287	417.78	417.78	417.78	125.00	330.00	330.00	330.00

[§] Due to the large station spacing, velocities above 50 m depth are not well resolved.

Table 1(b): Instrument groupings used to obtain 1D shear-wave velocity soundings along Line 1, model 2 (see Figure 2 for location). Average velocities to 10-, 30-, 50-, and 100-meter depths, denoted Vs10[§], Vs30[§], Vs50, and Vs100, respectively are listed along with the depths where the shear velocity first exceeds 0.5 km/s, 1.0 km/s, 1.5 km/s, and 2.0 km/s (Z0.5, Z1.0, Z1.5, and Z2.0 respectively).

Station Spread	Midpoint		Velocity, m/s			Depth, m			
	Latitude	Longitude	Vs30[§]	Vs50	Vs100	Z0.5	Z1.0	Z1.5	Z2.0
Line1 01 to 30	39.5276	-119.7462	366.86	366.86	396.36	75.90	332.50	332.50	332.50
Line1 02 to 31	39.5276	-119.7455	366.86	366.86	387.83	82.50	347.50	347.50	347.50
Line1 03 to 32	39.5276	-119.7450	366.86	366.86	387.83	82.50	347.50	347.50	347.50
Line1 05 to 34	39.5276	-119.7438	366.86	366.86	387.83	82.50	347.50	347.50	347.50
Line1 07 to 36	39.5276	-119.7426	338.57	338.57	391.80	62.50	347.50	347.50	347.50
Line1 09 to 38	39.5276	-119.7415	338.57	338.57	387.74	65.00	347.50	347.50	347.50
Line1 11 to 40	39.5276	-119.7403	338.57	338.57	387.74	65.00	347.50	347.50	347.50
Line1 13 to 42	39.5275	-119.7391	349.88	349.88	389.76	70.00	292.50	292.50	292.50
Line1 15 to 44	39.5275	-119.7380	372.52	372.52	402.55	75.00	277.50	277.50	277.50
Line1 17 to 46	39.5275	-119.7368	406.47	406.47	413.74	92.50	277.50	277.50	277.50
Line1 19 to 48	39.5274	-119.7357	400.81	400.81	438.42	65.00	285.00	285.00	285.00
Line1 21 to 50	39.5274	-119.7345	423.44	423.44	434.44	87.50	332.50	332.50	332.50
Line1 23 to 52	39.5273	-119.7333	406.47	406.47	423.86	82.50	342.50	342.50	342.50
Line1 25 to 54	39.5273	-119.7322	397.56	397.56	441.97	60.00	342.50	342.50	342.50
Line1 27 to 56	39.5274	-119.7310	397.56	397.56	418.59	80.00	342.50	342.50	342.50
Line1 29 to 58	39.5274	-119.7299	397.56	397.56	418.59	80.00	342.50	342.50	342.50
Line1 31 to 60	39.5274	-119.7287	397.56	397.56	418.59	80.00	342.50	342.50	342.50

[§] Due to the large station spacing, velocities above 50 m depth are not well resolved.

Table 2(a): Instrument groupings used to obtain 1D shear-wave velocity soundings along Line 2, Model 1 (see Figure 2 for location). Average velocities to 10-, 30-, 50-, and 100-meter depths, denoted Vs10[§], Vs30[§], Vs50, and Vs100, respectively are listed along with the depths where the shear velocity first exceeds 0.5 km/s, 1.0 km/s, 1.5 km/s, and 2.0 km/s (Z0.5, Z1.0, Z1.5, and Z2.0 respectively).

Station Spread	Midpoint		Velocity, m/s			Depth, m			
	Latitude	Longitude	Vs30[§]	Vs50	Vs100	Z0.5	Z1.0	Z1.5	Z2.0
Line2 01 to 30	39.5127	-119.8204	383.83	399.09	449.73	42.50	275.00	567.50	567.50
Line2 03 to 32	39.5127	-119.8192	366.86	401.53	451.28	42.50	215.00	550.00	550.00
Line2 04 to 33	39.5127	-119.8186	366.86	401.53	451.28	35.00	285.00	537.50	537.50
Line2 05 to 34	39.5127	-119.8180	423.44	435.05	480.50	42.50	397.50	505.00	505.00
Line2 07 to 36	39.5128	-119.8168	423.44	435.05	480.50	42.50	412.50	505.00	505.00
Line2 09 to 38	39.5129	-119.8157	468.71	468.71	503.60	50.00	392.50	520.00	520.00
Line2 11 to 40	39.5129	-119.8146	480.02	480.02	503.41	50.00	392.50	520.00	520.00
Line2 13 to 42	39.5129	-119.8134	485.68	485.68	517.41	50.00	392.50	520.00	520.00
Line2 15 to 44	39.5125	-119.8123	485.68	485.68	517.41	50.00	392.50	520.00	520.00
Line2 17 to 46	39.5124	-119.8111	485.68	485.68	517.41	50.00	392.50	520.00	520.00
Line2 19 to 48	39.5124	-119.8099	497.00	497.00	523.76	50.00	375.00	495.00	495.00
Line2 21 to 50	39.5125	-119.8087	497.00	497.00	523.76	50.00	375.00	495.00	495.00
Line2 22 to 51	39.5125	-119.8081	497.00	497.00	523.76	50.00	375.00	495.00	495.00
Line2 23 to 52	39.5125	-119.8075	497.00	497.00	536.10	50.00	375.00	435.00	435.00
Line2 25 to 54	39.5127	-119.8064	559.24	559.24	559.24	172.50	402.50	402.50	402.50
Line2 27 to 56	39.5128	-119.8052	559.24	559.24	559.24	172.50	402.50	402.50	402.50
Line2 29 to 58	39.5128	-119.8041	564.90	564.90	564.90	152.50	402.50	402.50	402.50
Line2 31 to 60	39.5129	-119.8030	564.90	564.90	564.90	152.50	355.00	355.00	355.00

[§] Due to the large station spacing, velocities above 50 m depth are not well resolved.

Table 2(b): Instrument groupings used to obtain 1D shear-wave velocity soundings along Line 2, Model 2 (see Figure 2 for location). Average velocities to 10-, 30-, 50-, and 100-meter depths, denoted Vs10[§], Vs30[§], Vs50, and Vs100, respectively are listed along with the depths where the shear velocity first exceeds 0.5 km/s, 1.0 km/s, 1.5 km/s, and 2.0 km/s (Z0.5, Z1.0, Z1.5, and Z2.0 respectively).

Station Spread	Midpoint		Velocity, m/s			Depth, m			
	Latitude	Longitude	Vs30[§]	Vs50	Vs100	Z0.5	Z1.0	Z1.5	Z2.0
Line2 01 to 30	39.5127	-119.8204	383.83	399.09	449.73	42.50	275.00	567.50	567.50
Line2 03 to 32	39.5127	-119.8192	366.86	401.53	451.28	42.50	215.00	550.00	550.00
Line2 04 to 33	39.5127	-119.8186	366.86	401.53	451.28	35.00	285.00	537.50	537.50
Line2 05 to 34	39.5127	-119.8180	423.44	435.05	480.50	42.50	397.50	505.00	505.00
Line2 07 to 36	39.5128	-119.8168	423.44	435.05	480.50	42.50	412.50	505.00	505.00
Line2 09 to 38	39.5129	-119.8157	468.71	468.71	503.60	50.00	392.50	520.00	520.00
Line2 11 to 40	39.5129	-119.8146	480.02	480.02	503.41	50.00	392.50	520.00	520.00
Line2 13 to 42	39.5129	-119.8134	485.68	485.68	517.41	50.00	392.50	520.00	520.00
Line2 15 to 44	39.5125	-119.8123	485.68	485.68	517.41	50.00	392.50	520.00	520.00
Line2 17 to 46	39.5124	-119.8111	485.68	485.68	517.41	50.00	392.50	520.00	520.00
Line2 19 to 48	39.5124	-119.8099	525.29	525.29	525.29	100.00	432.50	432.50	432.50
Line2 21 to 50	39.5125	-119.8087	525.29	525.29	525.29	112.50	432.50	432.50	432.50
Line2 22 to 51	39.5125	-119.8081	525.29	525.29	525.29	112.50	437.50	437.50	437.50
Line2 23 to 52	39.5125	-119.8075	525.29	525.29	525.29	105.00	370.00	370.00	370.00
Line2 25 to 54	39.5127	-119.8064	553.58	553.58	553.58	117.50	370.00	370.00	370.00
Line2 27 to 56	39.5128	-119.8052	553.58	553.58	553.58	117.50	370.00	370.00	370.00
Line2 29 to 58	39.5128	-119.8041	564.90	564.90	564.90	120.00	372.50	372.50	372.50
Line2 31 to 60	39.5129	-119.8030	564.90	564.90	564.90	115.00	330.00	330.00	330.00

[§] Due to the large station spacing, velocities above 50 m depth are not well resolved.

Table 2(c): Instrument groupings used to obtain 1D shear-wave velocity soundings along Line 2, Model 3 (see Figure 2 for location). Average velocities to 10-, 30-, 50-, and 100-meter depths, denoted Vs10[§], Vs30[§], Vs50, and Vs100, respectively are listed along with the depths where the shear velocity first exceeds 0.5 km/s, 1.0 km/s, 1.5 km/s, and 2.0 km/s (Z0.5, Z1.0, Z1.5, and Z2.0 respectively).

Station Spread	Midpoint		Velocity, m/s			Depth, m			
	Latitude	Longitude	Vs30[§]	Vs50	Vs100	Z0.5	Z1.0	Z1.5	Z2.0
Line20 1 to 30	39.5127	-119.8204	383.83	399.09	449.73	42.50	275.00	567.50	567.50
Line2 03 to 32	39.5127	-119.8192	366.86	401.53	451.28	42.50	215.00	550.00	550.00
Line2 04 to 33	39.5127	-119.8186	366.86	401.53	451.28	35.00	285.00	537.50	537.50
Line2 05 to 34	39.5127	-119.8180	423.44	435.05	480.50	42.50	397.50	505.00	505.00
Line2 07 to 36	39.5128	-119.8168	423.44	435.05	480.50	42.50	412.50	505.00	505.00
Line2 09 to 38	39.5129	-119.8157	468.71	468.71	503.60	50.00	392.50	520.00	520.00
Line2 11 to 40	39.5129	-119.8146	480.02	480.02	503.41	50.00	392.50	520.00	520.00
Line2 13 to 42	39.5129	-119.8134	485.68	485.68	517.41	50.00	392.50	520.00	520.00
Line2 15 to 44	39.5125	-119.8123	485.68	485.68	517.41	50.00	392.50	520.00	520.00
Line2 17 to 46	39.5124	-119.8111	485.68	485.68	517.41	50.00	392.50	520.00	520.00
Line2 19 to 48	39.5124	-119.8099	497.00	497.00	523.76	50.00	375.00	495.00	495.00
Line2 21 to 50	39.5125	-119.8087	497.00	497.00	523.76	50.00	375.00	495.00	495.00
Line2 22 to 51	39.5125	-119.8081	497.00	497.00	523.76	50.00	375.00	495.00	495.00
Line2 23 to 52	39.5125	-119.8075	525.29	525.29	525.29	105.00	370.00	370.00	370.00
Line2 25 to 54	39.5127	-119.8064	553.58	553.58	553.58	117.50	370.00	370.00	370.00
Line2 27 to 56	39.5128	-119.8052	553.58	553.58	553.58	117.50	370.00	370.00	370.00
Line2 29 to 58	39.5128	-119.8041	564.90	564.90	564.90	120.00	372.50	372.50	372.50
Line2 31 to 60	39.5129	-119.8030	564.90	564.90	564.90	115.00	330.00	330.00	330.00

[§] Due to the large station spacing, velocities above 50 m depth are not well resolved.

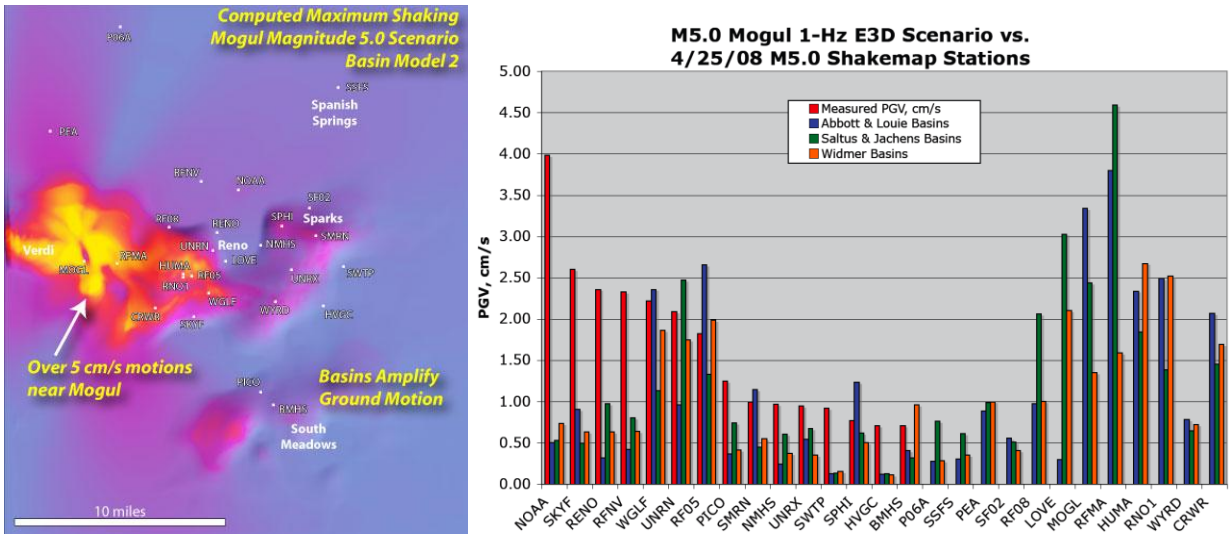

Figure 1: Results of a trial 3D scenario model of the M5 4/25/08 Mogul main shock, computed to a maximum frequency of 1.0 Hz. (left) Peak ground velocity (PGV) map resulting from the Nevada ShakeZoning community seismic modeling environment, with Abbott and Louie (2000) basin structure in shaded relief. (right) PGV recorded at named stations (red bars), not matched by Nevada ShakeZoning 3D predictions using 3 different basin models.

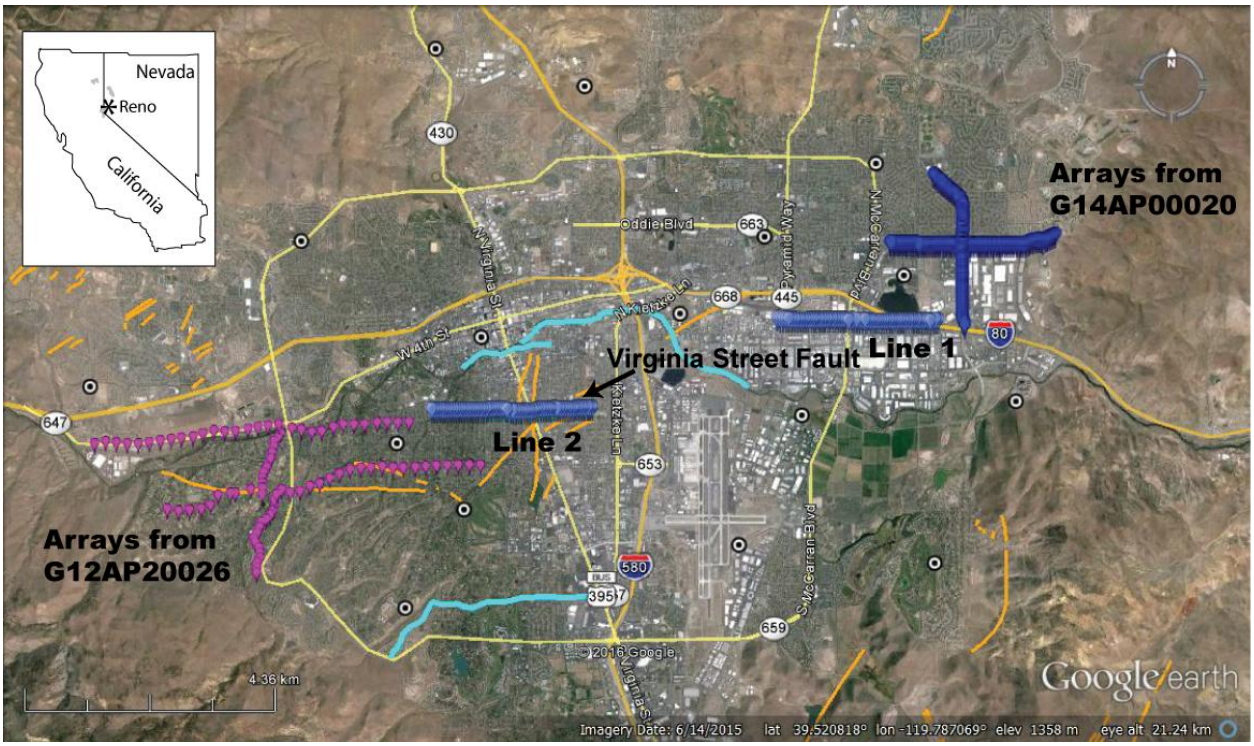

Figure 2(a): Locations of the two 2015 deep refraction microtermor (ReMi) arrays are shown in purple (Line 1) and green (Line 2). These new lines complement data acquired across the deepest portions of the basin (see Figure 2) under grants G12AP20026 (magenta, light blue, and white). Sixty wireless instruments were deployed at 50 m spacing along the 2.95 km long arrays to record ambient noise. Reflection lines acquired by Stephenson *et al.* (2013) and Frary (2012) along the Truckee River are shown in cyan. ANSS station locations (white dots) are also shown. The two northwestern arrays for this study, Line 1 and Line 2, are shown in detail in Figure 2(b). Inset shows the geographic location of Reno, Nevada, U.S.A.

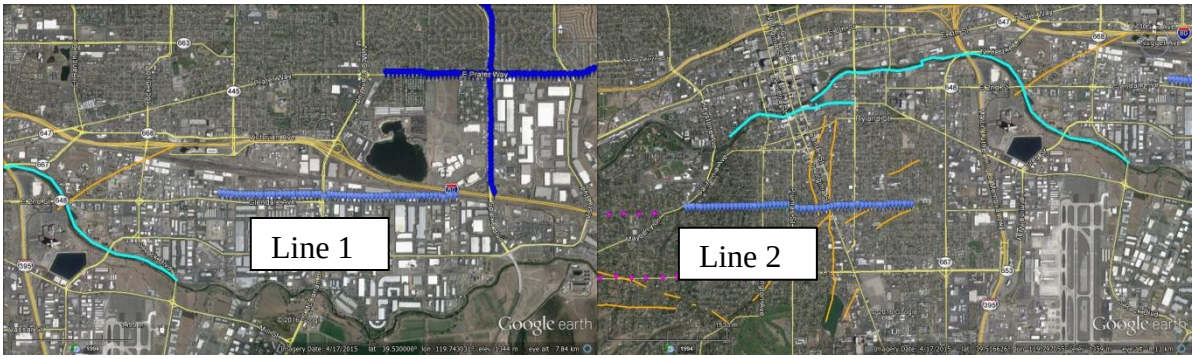

Figure 2(b): Locations of two deep refraction microtermor (ReMi) arrays acquired in 2015 are shown: Line 1 (right) and Line 2 (left). Sixty wireless instruments were deployed at 50 m spacing along the 2.95 km long arrays to record ambient noise.

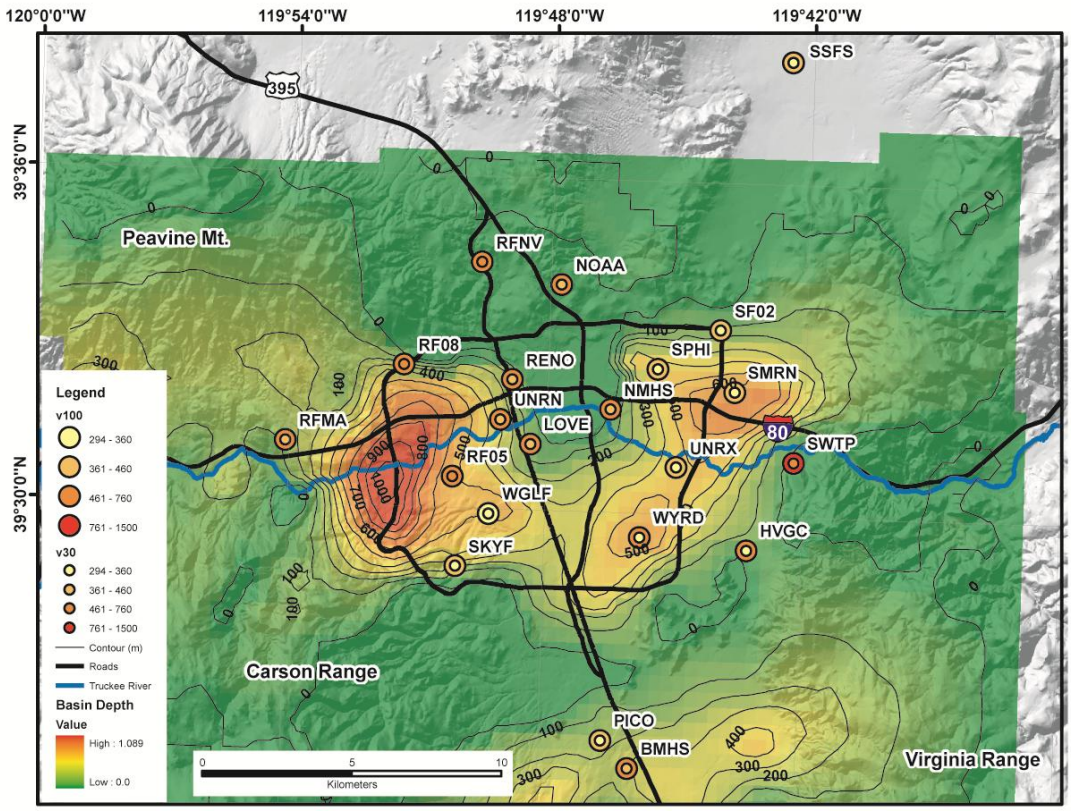

Figure 3: Basin depth model from Abbott and Louie (2000), based on gravity observations. Contours are 100 m. The formal name for the area is the Central Truckee Meadows, referring to the geomorphic flat region of Quaternary deposits. We refer to it as the Reno area basin after the largest city in the Reno–Sparks urban area, following Abbott and Louie (2000), incorporating both the geophysical and geomorphic expression of the basin.

Figure 4: Pictures showing the Sigma™ cableless acquisition system by iSeis (Heath,2011). Each is powered by a 12-V battery and is connected to a single vertical P-wave geophone for this study.

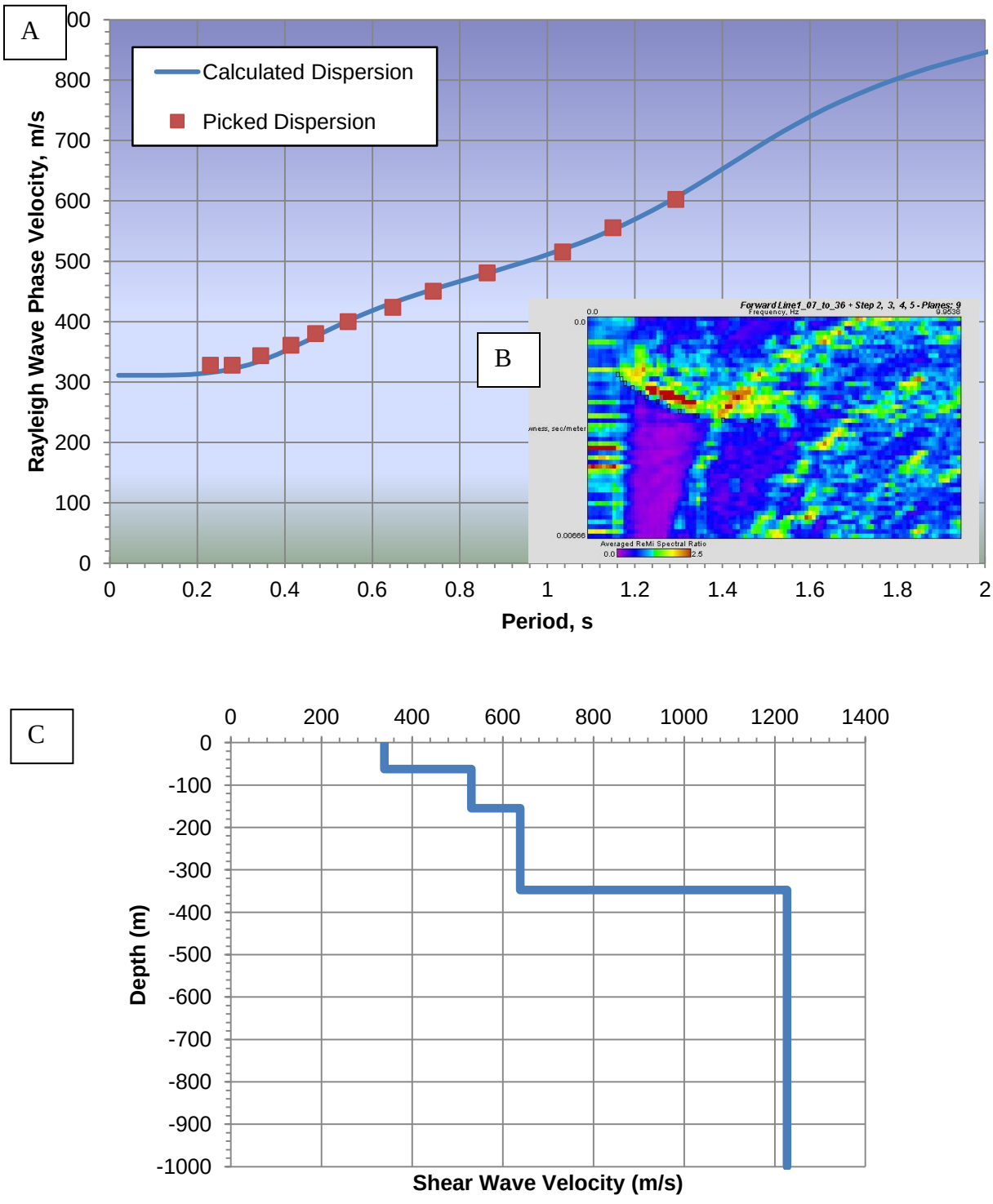

Figure 5: Example of ReMi analysis for a sample record along Line 1 7-36, model 2. Recorded microtremor data are first transformed into the frequency-slowness domain (Louie, 2001) **(A)**. The dispersion curve is then picked **(B)** and modeled to obtain a 1D shear-wave velocity profile **(C)**.

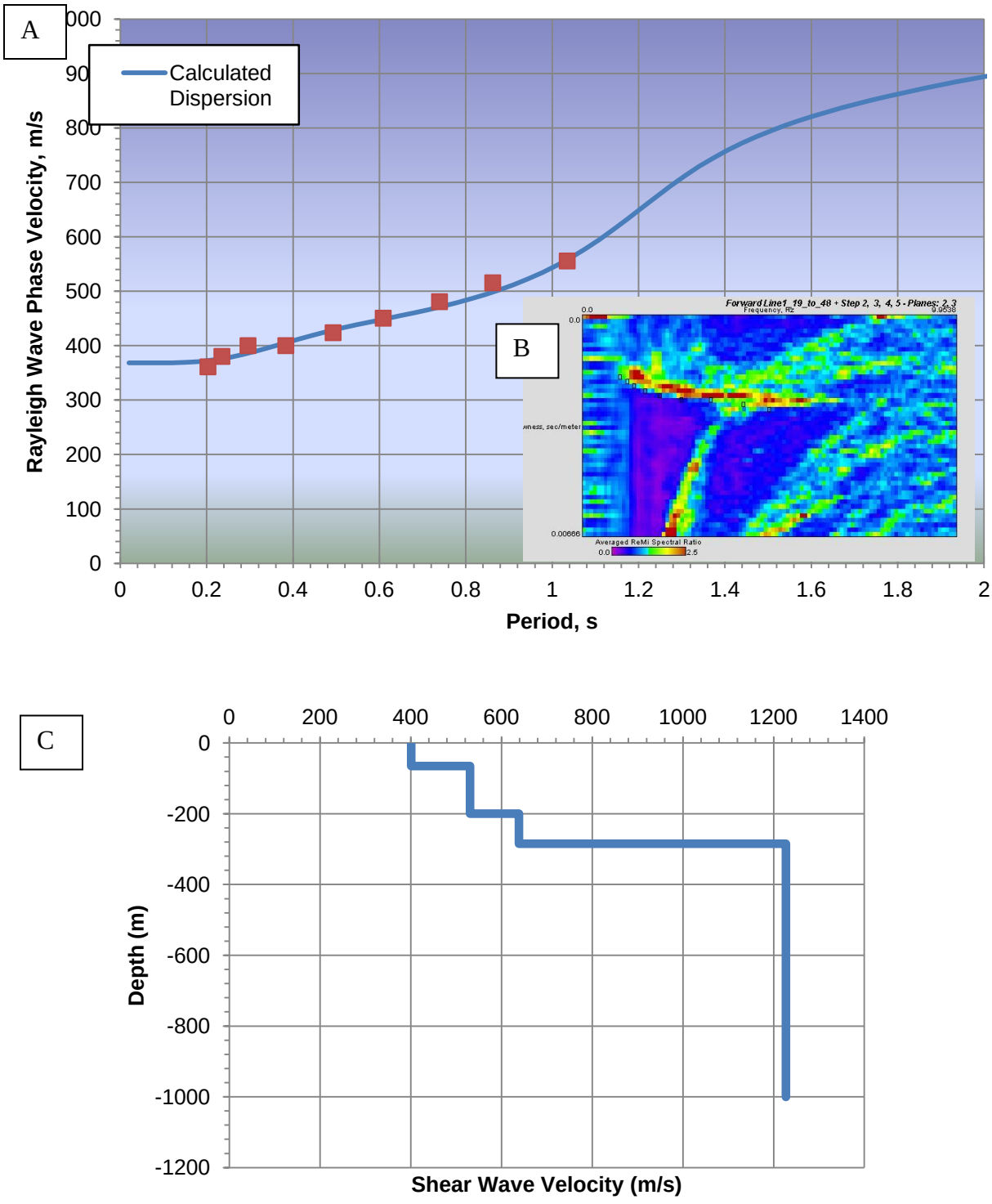

Figure 6: Example of ReMi analysis for a sample record along Line 1 19-48, model 2. Recorded microtremor data are first transformed into the frequency-slowness domain (Louie, 2001) **(A)**. The dispersion curve is then picked **(B)** and modeled to obtain a 1D shear-wave velocity profile **(C)**.

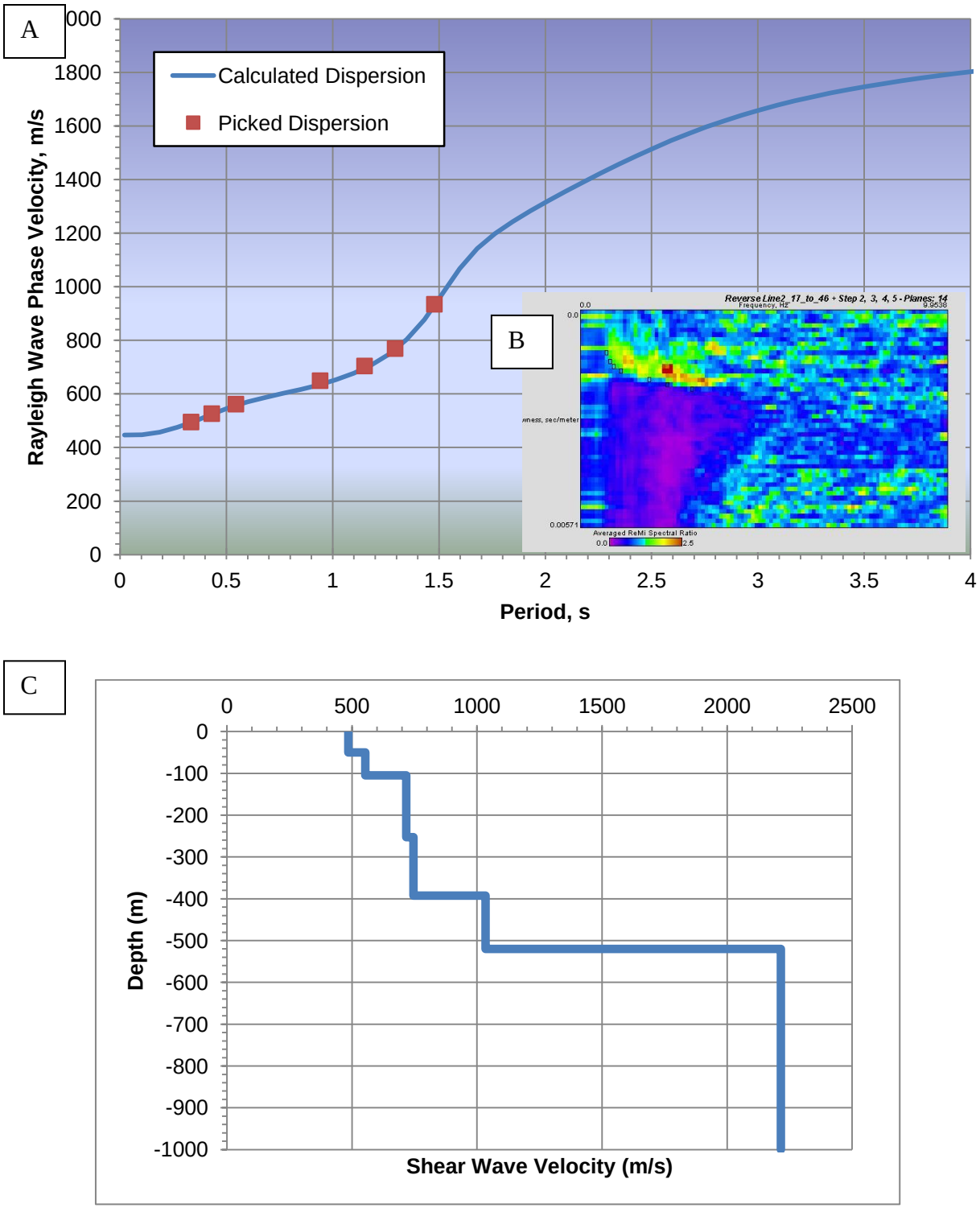

Figure 7: Example of ReMi analysis for a sample record along Line 2 17-46, Model 2. Recorded microtremor data are first transformed into the frequency-slowness domain (Louie, 2001) **(A)**. The dispersion curve is then picked **(B)** and modeled to obtain a 1D shear-wave velocity profile **(C)**.

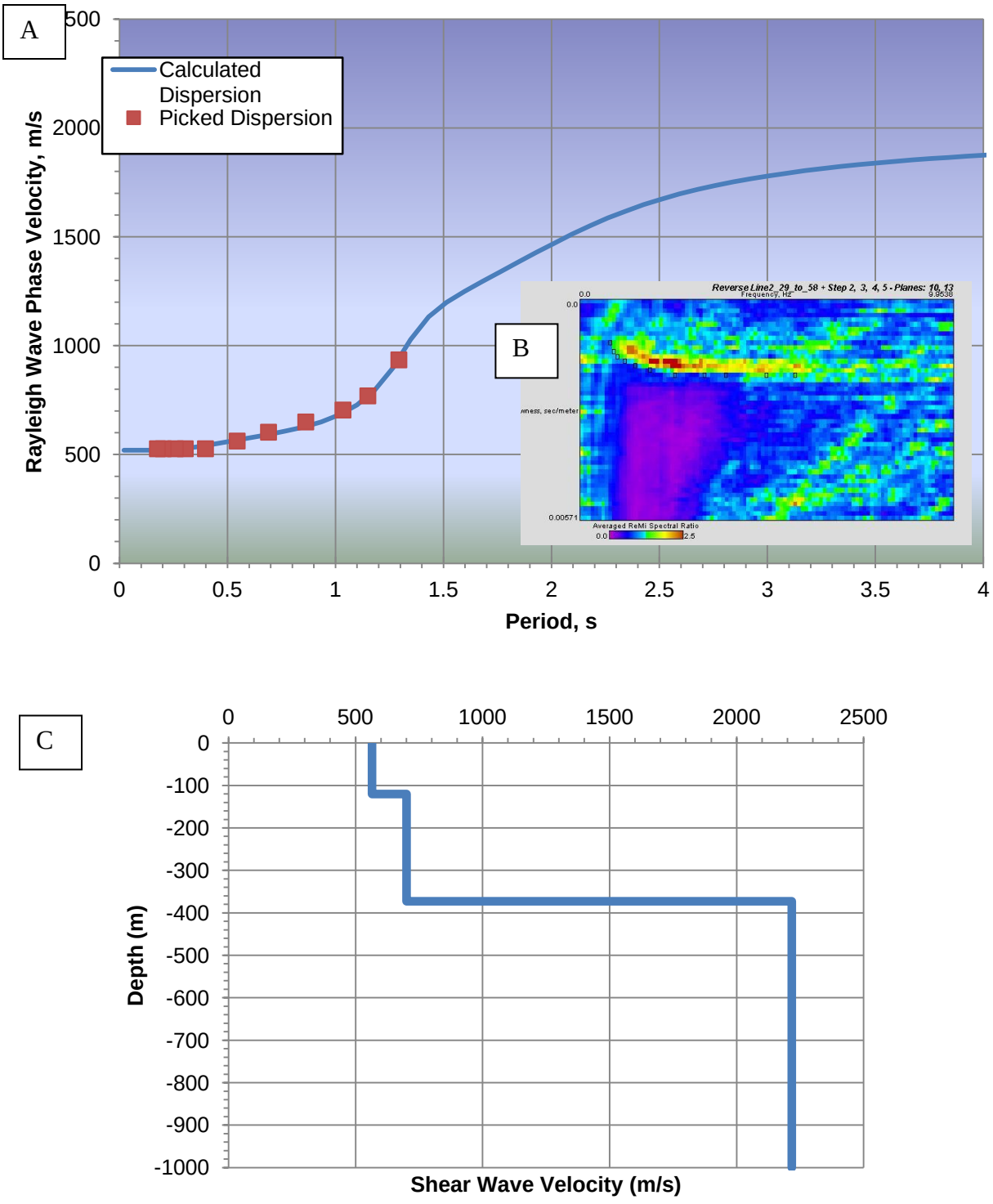

Figure 8: Example of ReMi analysis for a sample record along Line 2 29-58, model 2. Recorded microtremor data are first transformed into the frequency-slowness domain (Louie, 2001) **(A)**. The dispersion curve is then picked **(B)** and modeled to obtain a 1D shear-wave velocity profile **(C)**.

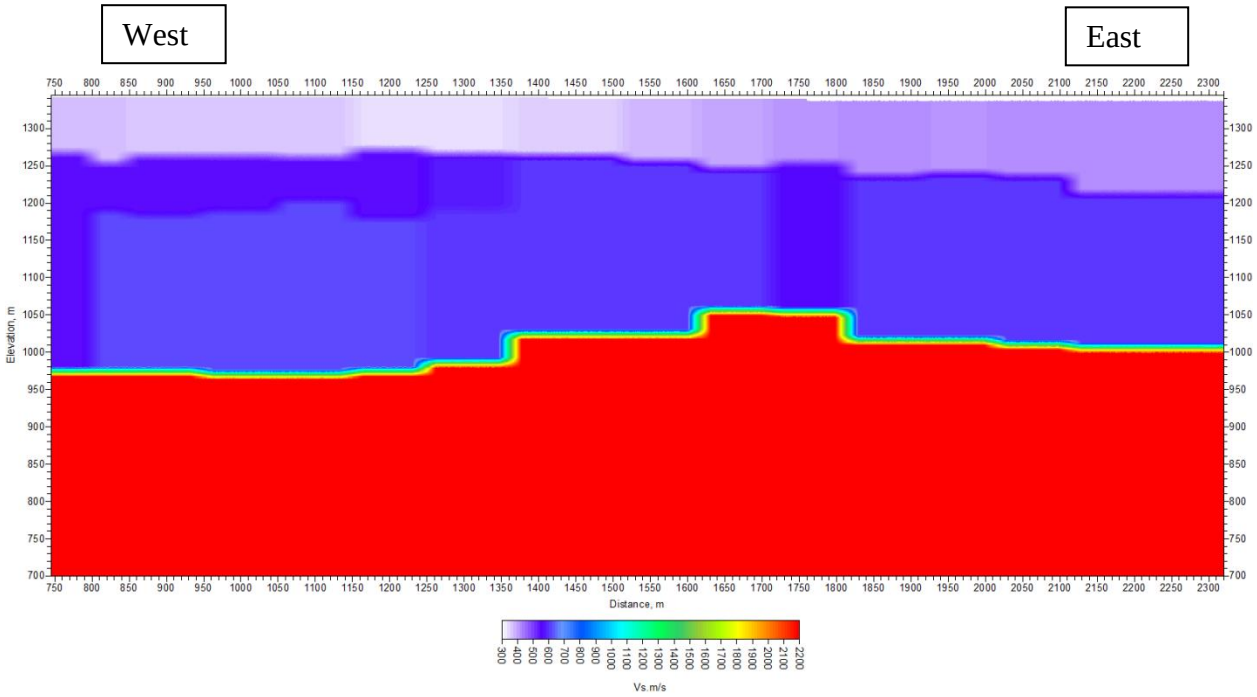

Figure 9: 2D Vs velocity modeled using 2D refraction microtremor analysis for Line 1, Model 1. The image is compiled through interpolation of 1D shear-velocity profiles as function of depth determined from a moving array of 30 instruments along each line length. Distances along the array (assuming Station 1 is located at 0 m) are show along the bottom.

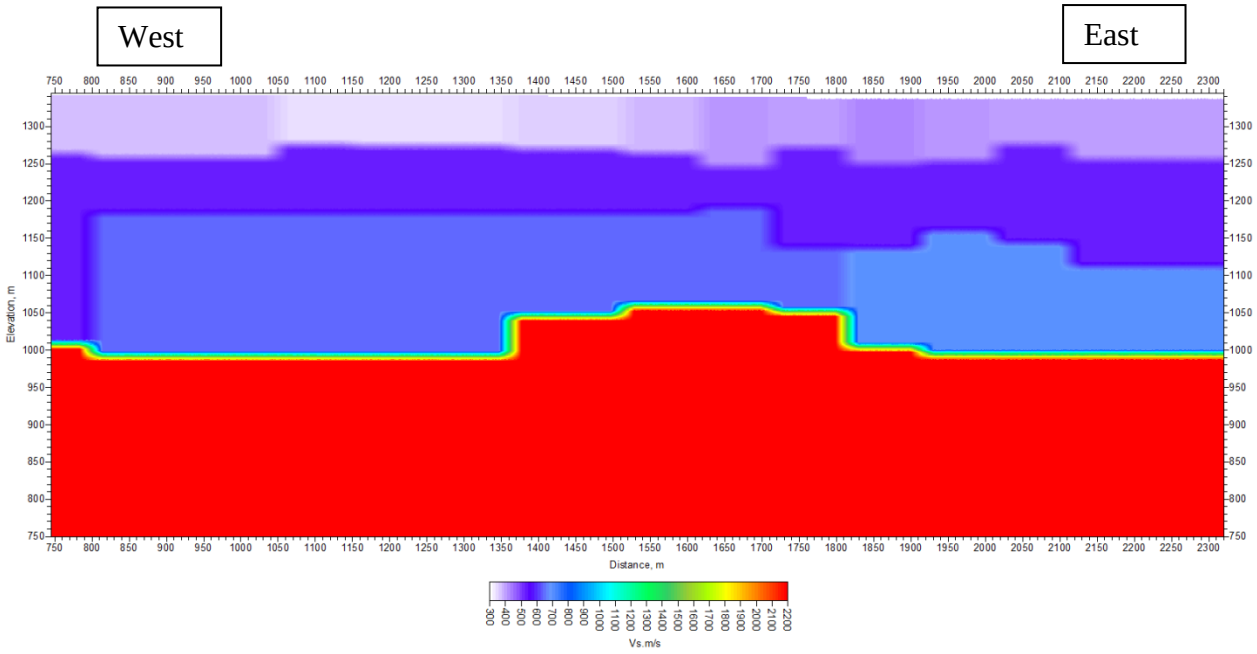

Figure 10: 2D Vs velocity modeled using 2D refraction microtremor analysis for Line 1, Model 2. The image is compiled through interpolation of 1D shear-velocity profiles as function of depth determined from a moving array of 30 instruments along each line length. Distances along the array (assuming Station 1 is located at 0 m) are show along the bottom.

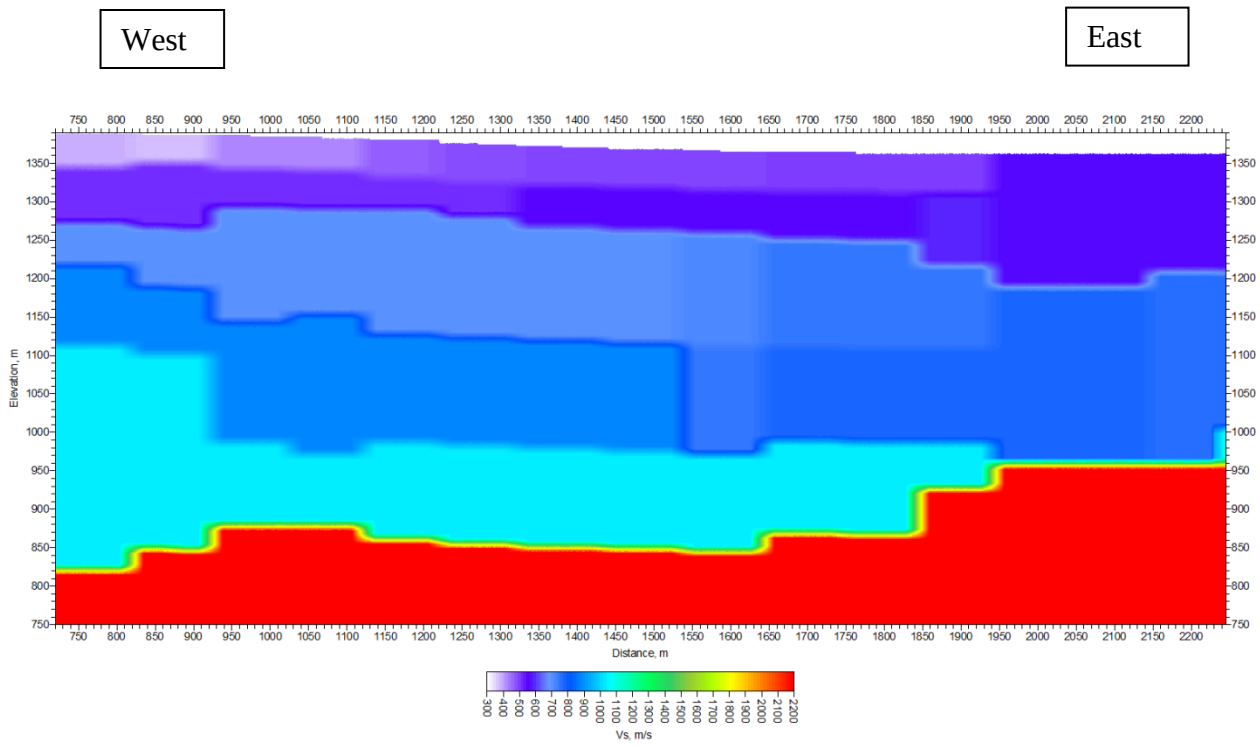

Figure 11: 2D Vs velocity modeled using 2D refraction microtremor analysis for Line 2, Model 1. The image is compiled through interpolation of 1D shear-velocity profiles as function of depth determined from a moving array of 30 instruments along each line length. Distances along the array (assuming Station 1 is located at 0 m) are show along the bottom.

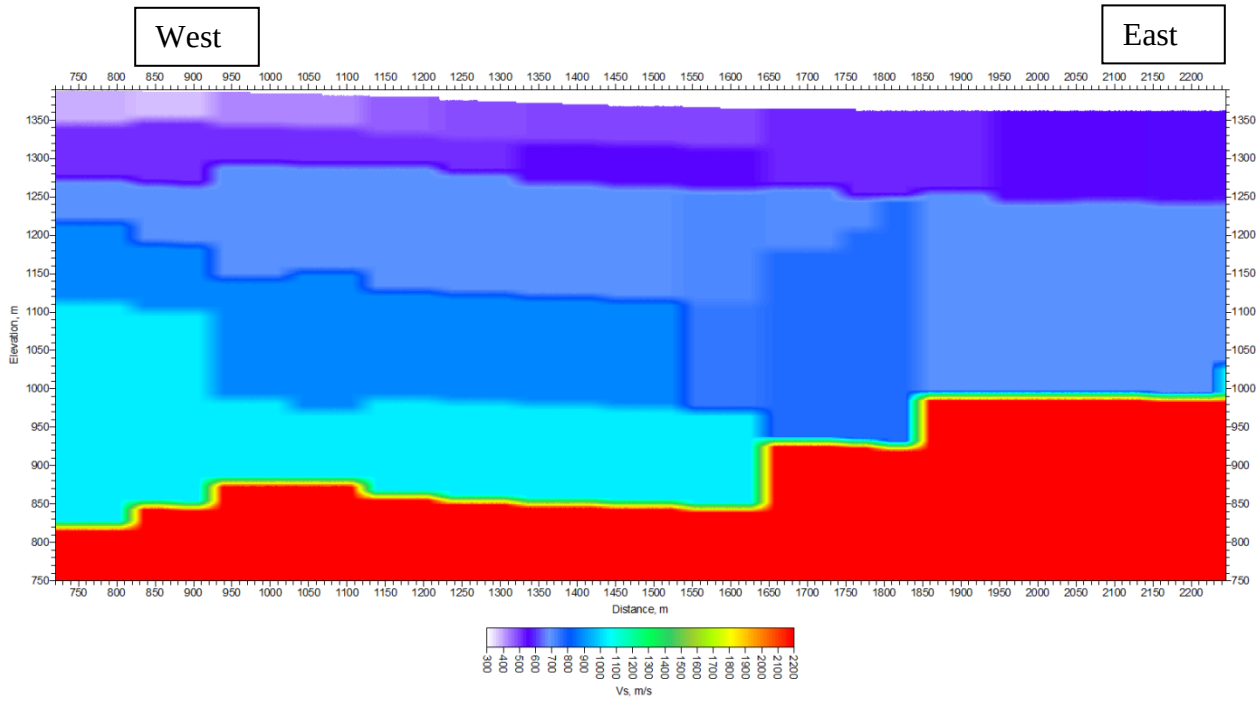

Figure 12: 2D Vs velocity modeled using 2D refraction microtremor analysis for Line 2, Model 2. The image is compiled through interpolation of 1D shear-velocity profiles as function of depth determined from a moving array of 30 instruments along each line length. Distances along the array (assuming Station 1 is located at 0 m) are show along the bottom.

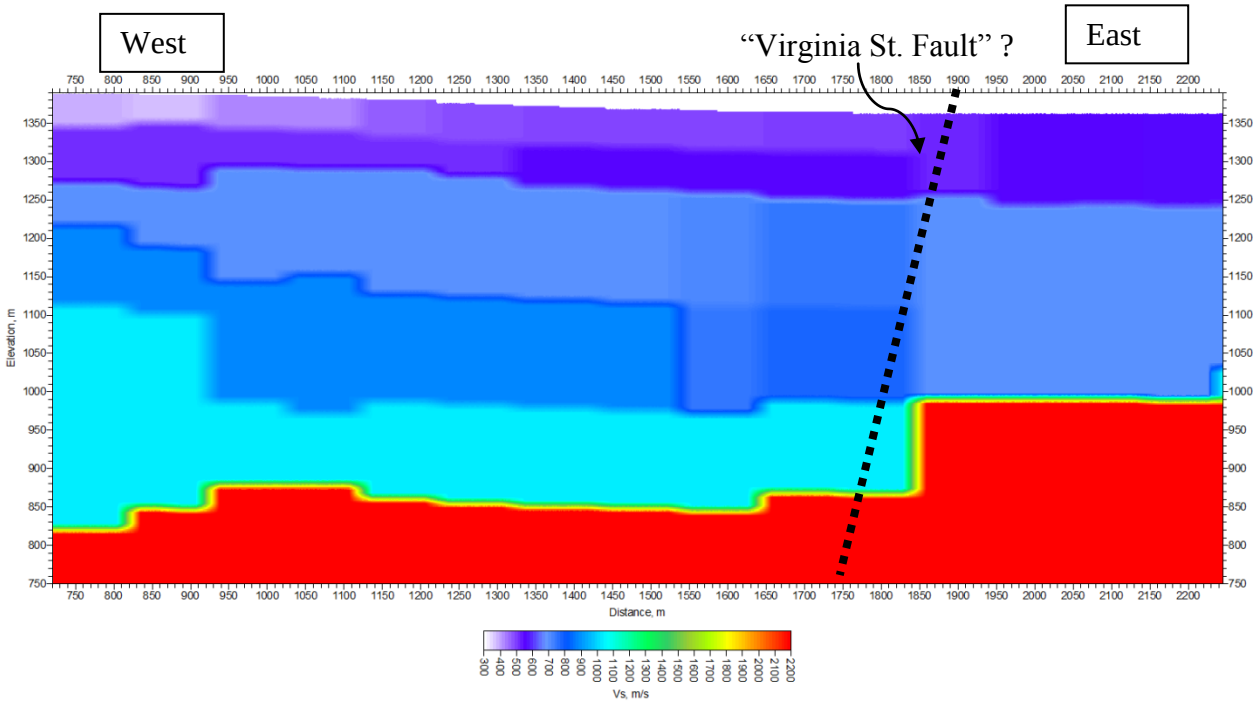

Figure 13: 2D Vs velocity modeled using 2D refraction microtremor analysis for Line 2, Model 3. The image is compiled through interpolation of 1D shear-velocity profiles as function of depth determined from a moving array of 30 instruments along each line length. Distances along the array (assuming Station 1 is located at 0 m) are show along the bottom.

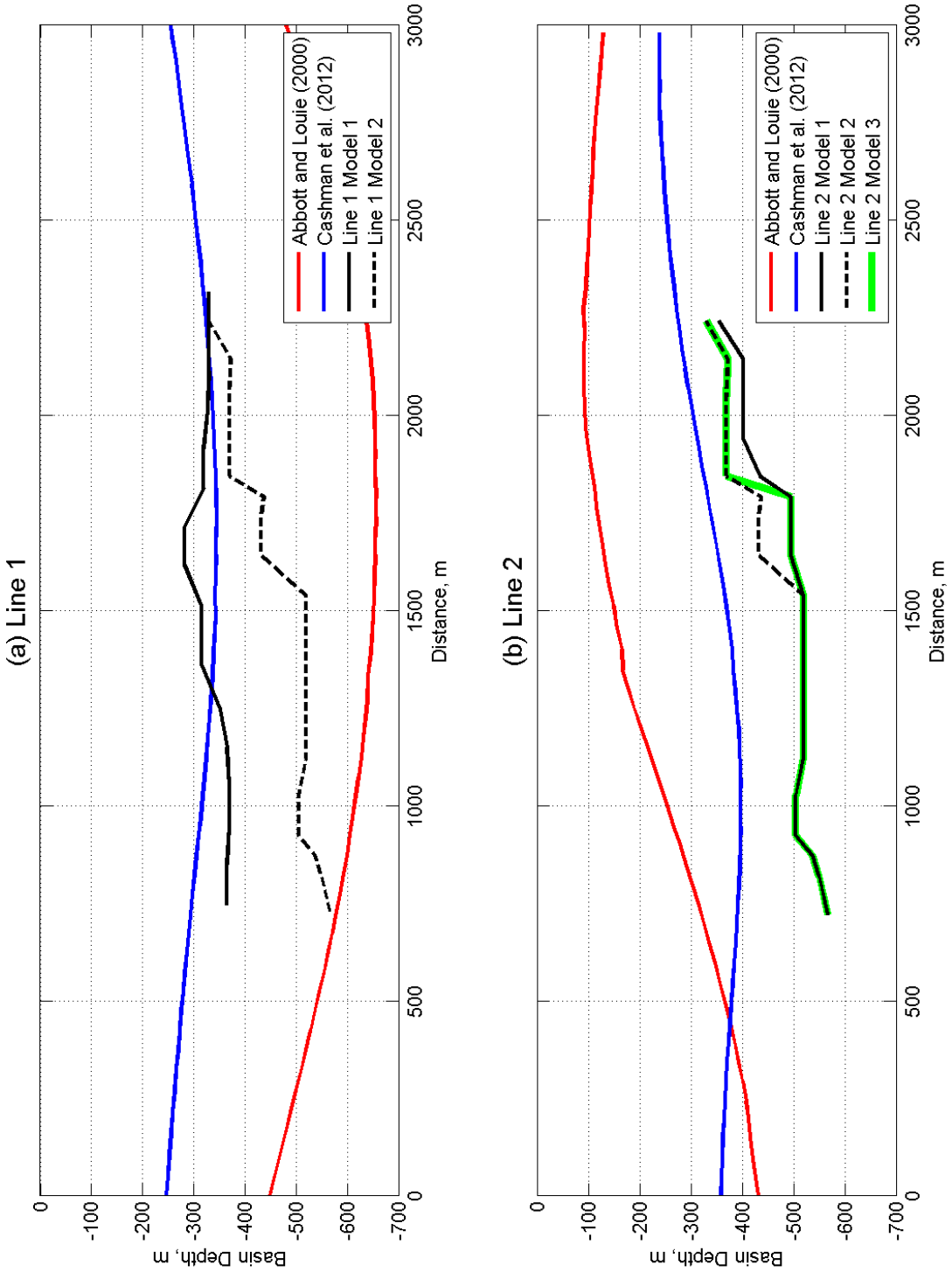

Figure 14: Comparison between basin depths from ReMi along (a) Line 1 and (b) Line 2, with those estimated from gravity by Abbott and Louie (2000) and Cashman *et al.* (2012) models. Differences between the Abbott and Louie and Cashman *et al.* 3D gravity-depth models may highlight differences in the assumed basements material, and their signifiance in terms of seismic response.

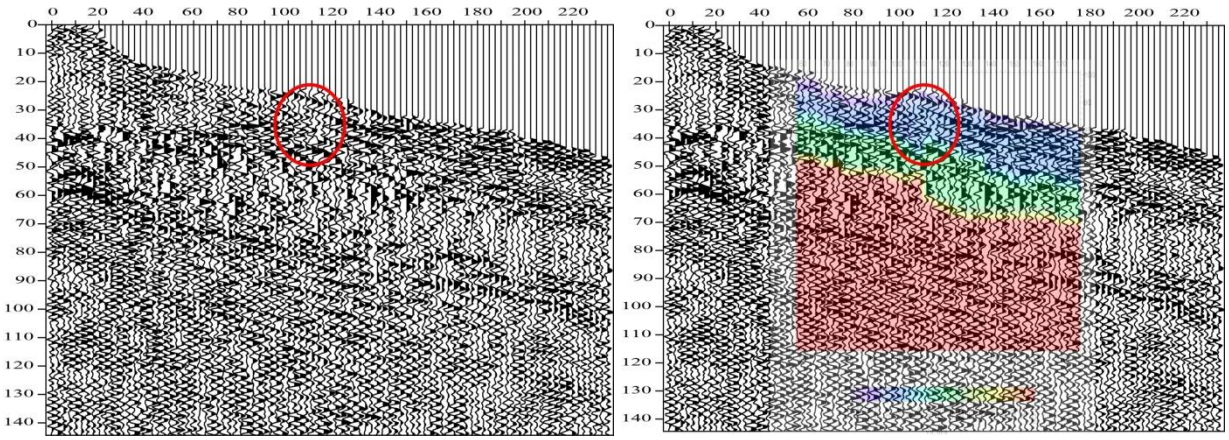

Figure 15: (a) A preliminary depth-migrated section of the interferometric shot gathers along the Hadfield Road (New Zealand) seismic array. (b) comparison with a 2-D S-wave velocity (Vs) model constructed using the moving array ReMi technique along the seismic array. The red cirle indicates the location of a presumed fault based on a 1948 air photo.